Penetration of Electromagnetic Fields Through an Elliptical Hole in a Wall of Finite Thickness

Branislav Radak and Robert L. Gluckstern

Abstract—**The penetration of electromagnetic fields through an elliptical hole of variable eccentricity in a wall of finite thickness is analyzed. Six cases are considered: $p \approx$ 0, 0.2, 0.4, 0.6, 0.8, 1., where $p = (a - b)/(a + b)$, a and b being semimajor and semiminor axes of the ellipse. Polarizabilities and susceptibilities are calculated. Results for zero-thickness wall are compared to known analytical expressions.**

I. Introduction

WHEN A charged particle beam traveling at relativistic velocity in a beam pipe passes a hole or a slot in the beam pipe wall, it generates an electromagnetic wakefield [1]–[3]. This wakefield acts back on the beam perturbing its motion. The wakefields lead to bunch lengthening and even instability, and they set a limit on the beam current that can be carried in the pipe. It is therefore important to determine the optimum design of holes and slots for purposes, such as pumping and beam position monitoring, and the extent to which these holes must be shielded from the beam.

Another motivation for studying the wakefield produced by a hole or slot is the recent experience in the Large Hadron Collider (LHC) and Superconducting Supercollider (SSC) designs [4], [5]. The energy radiated by the circulating protons is sufficient to cause an excessive heat load on, and unwanted secondary emissions from, the beam pipe that will be at liquid helium temperatures. These groups are now exploring the use of a liner at liquid nitrogen temperature in which there are many small holes to provide an adequate vacuum for the beam. The wakefields caused by these holes must be kept sufficiently small so as not to disturb the beam significantly.

Let us consider the wakefields of a point charge in a circular beam pipe with a small hole in the wall. In frequency space these wakefields are the frequency dependent longitudinal and transverse coupling impedances [6]. For holes whose dimensions are small compared to the wavelength, the impedances are obtained from the solutions for the penetration of the static electric and magnetic fields through the holes. Specifically, one obtains the induced electric and magnetic dipole moments and defines a polarizability and two susceptibilities that depend only on the shape and size of the hole. These quantities were first calculated analytically by Bethe [7] for a circular and an elliptical hole in a wall of zero thickness. For other shapes, or for a wall with finite thickness, numerical methods are necessary.

Both the longitudinal and transverse impedances depend on $\psi - \chi$, the difference between the susceptibility and the polarizability. Using the Bethe result for an elliptical slot in a wall of zero thickness, one sees that ψ and χ approach each other as the slot lengthens in the direction of the beam (and becomes narrower in the direction perpendicular to the beam). This is understandable since the image currents on the wall will be less disturbed by the slot. Moreover, for a long slot the geometry becomes two-dimensional and $\psi - \chi \to 0$, since the electric and magnetic results can be obtained from the same conformal transformation.

The finite thickness of the wall forces one to use a numerical approach. In this work we follow the analysis of Gluckstern and Diamond [8] for a circular hole in a wall of finite thickness. They constructed a variational formulation for both the polarizability and susceptibility and obtained accurate numerical values by using truncated expansions for the unknown fields or potentials. In addition they separated each calculation into a symmetric and asymmetric part, finally obtaining both "inside" and "outside" polarizabilities and susceptibilities. The penetration of the fields into the region outside the hole depends only on ψ_{out} and χ_{out}. And, if there are no appreciable fields in the region outside the hole, the impedances depends only on $\psi_{\text{in}} - \chi_{\text{in}}$. In the present work we try to calculate $\chi_{\text{in}} = \chi_s + \chi_a$, $\chi_{\text{out}} = \chi_s - \chi_a$, $\psi_{\text{in}} = \psi_s + \psi_a$, $\psi_{\text{out}} = \psi_s - \psi_a$ for an elliptical hole in a wall of finite thickness. The subscripts "s" and "a" refer to the symmetric and antisymmetric configurations for the potentials.

II. General Consideration for Finite Wall Thickness

The hole in the pipe is of elliptic shape with semimajor and semiminor axes a and b and with the focal length $c(c^2 = a^2 - b^2)$ and thickness L. Electric field in the vicinity of the hole must be perpendicular to the wall, while the magnetic field is to be parallel.

A. Electric Case

The electric field is decomposed into a symmetric and antisymmetric geometry as shown in Fig. 1. The coordinate origin in the middle of the hole, so that the wall surfaces are at $z = \pm L/2$. Since no charges are present we have to solve Laplace equation for the potential

$$\nabla^2\Phi(x, y, z) = \frac{\partial^2\Phi}{\partial x^2} + \frac{\partial^2\Phi}{\partial y^2} + \frac{\partial^2\Phi}{\partial z^2} = 0. \qquad (2.1)$$

Manuscript received December 10, 1993; revised March 11, 1994. This work was supported in part by U.S. Department of Energy.

The authors are with the Department of Physics and Astronomy, University of Maryland at College Park, College Park, MD 20742-411 USA.

IEEE Log Number 9406796.

The general solution for the symmetric part of the potential in the regions $|z| > L/2$ and $|z| < L/2$ can be written in the form:

$$\Phi^s_{\text{out}}(\vec{r},z) = (E/2)(|z| - L/2) + \int d\vec{\sigma} a(\vec{\sigma}) e^{i\vec{\sigma}\cdot\vec{r} - \sigma(|z|-L/2)}$$

$$\Phi^s_{\text{in}}(\vec{r},z) = \sum_{m,n} D_{m,n}\Phi_{m,n}(\vec{r}) \frac{\cosh(\gamma_{m,n}z)}{\cosh(\frac{1}{2}\gamma_{m,n}L)}. \tag{2.2}$$

Here, we have $\vec{\sigma} = (\sigma_1\vec{i} + \sigma_2\vec{j})$, $\sigma = \sqrt{\sigma_1^2 + \sigma_2^2}$ and $a(\vec{\sigma})$ is to be determined. $\Phi_{m,n}(\vec{r})$ is a complete set of appropriate trial functions that we will have to choose judiciously, and $\gamma_{m,n}$ is the set of eigenvalues of the two-dimensional (orthogonal) Laplacian

$$\nabla^2\Phi_{m,n} + \gamma^2_{m,n}\Phi_{m,n} = 0.$$

These functions must satisfy the condition $\Phi_{m,n}$ (boundary) $= 0$, as well as orthonormality conditions

$$\int d\vec{r}\Phi_{m,n}(\vec{r})\Phi_{p,q}(\vec{r}) = \delta_{mp}\delta_{nq}$$

If we now define

$$f(\vec{r}) \equiv \Phi^s(\vec{r}, L/2) = \int d\vec{\sigma} a(\vec{\sigma}) e^{i\vec{\sigma}\cdot\vec{r}},$$

we easily get

$$a(\vec{\sigma}) = \frac{1}{4\pi^2}\int d\vec{r} e^{-i\vec{\sigma}\cdot\vec{r}} f(\vec{r})$$

$$D_{m,n} = \int d\vec{r}\Phi_{m,n}(\vec{r}) f(\vec{r}). \tag{2.3}$$

If we now match the derivatives of the potential at $z = L/2$ and use (2.3), we get

$$\int d\vec{r} f(\vec{r}) K(\vec{r},\vec{r}\,') = E/2, \tag{2.4}$$

where

$$K(\vec{r},\vec{r}\,') = \frac{1}{4\pi^2}\int d\vec{\sigma}\sigma e^{i(\vec{r}-\vec{r}\,')}\cdot\vec{\sigma} + \sum_{m,n}\gamma_{m,n}\tanh\left(\frac{1}{2}\gamma_{m,n}L\right)\Phi_{m,n}(\vec{r})\Phi_{m,n}(\vec{r}\,').$$

The kernel K is real and symmetric. To get the variational form for the polarizability, we start with its definition:

$$\chi_s \equiv \frac{2}{E}\int d\vec{r} f(\vec{r}),$$

and then multiply (2.4) by $f(\vec{r}')$ and integrate over the hole. One then obtains

$$\chi_s^{-1} = \frac{\int d\vec{r} d\vec{r}\,' f(\vec{r}) K(\vec{r},\vec{r}\,') f(\vec{r}\,')}{[\int d\vec{r} f(\vec{r})]^2}. \tag{2.5}$$

This is the general variational form for the polarizability for the symmetric potential. The antisymmetric case has a sinh function instead of a cosh in (2.2). Formulas derived so far are valid for any geometry. We now turn our attention to elliptical geometry and compare the elliptical coordinates and "angular" and "radial" functions with their cylindrical counterparts (see Appendix):

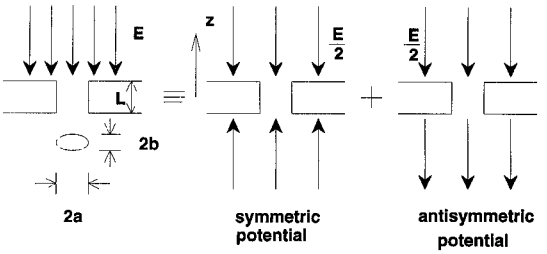

Fig. 1. An electric field perpendicular to the wall is split into symmetric and antisymmetric components.

	Elliptical case	Cylindrical case
	$x = c\cosh(\xi)\cos(\eta)$,	$x = r\cos(\phi)$
	$y = c\sinh(\xi)\sin(\eta)$,	$y = r\sin(\phi)$
	$z = z$,	$z = z$
"Angular" function	$\text{Se}_{2m,n}(h_{2m,n},\eta)$	$\cos(2m\phi)$
"Radial" function	$\text{Je}_{2m,n}(h_{2m,n},\xi)$	$J_{2m}(p_n r/a)$

where $J_{2m}(p_n) = 0$. The constant c in the previous formula is the eccentricity of the ellipse. We also have $a = c\cosh\xi_0$, $b = c\sinh\xi_0$, where a and b are the semimajor and semiminor axes of the ellipse, and ξ_0 is the value of the "radial" coordinate ξ at the wall surface of the hole. The dependence of the "angular" function on the radial index n, occurring in the elliptical case, contributes greatly to the analytic and numerical complications in the present analysis.

The Laplace equation in elliptical coordinates has the following form:

$$\nabla^2\Phi(x,y,z) = \frac{1}{c^2(\cosh^2\xi - \cos^2\eta)} \times \left(\frac{\partial^2\Phi}{\partial\xi^2} + \frac{\partial^2\Phi}{\partial\eta^2} + \frac{\partial^2\Phi}{\partial z^2}\right) = 0, \tag{2.6}$$

and we look for the solution in the form $\Phi(x,y,z) = F(\xi)\,G(\eta)\,Z(z)$ in which case the Laplace equation splits into the following three equations:

$$\frac{d^2Z}{dz^2} = k^2 Z(z),$$

$$\frac{d^2F}{d\xi^2} = (\tilde{b} - h^2\cosh^2\xi)F(\xi), \tag{2.7a,b,c}$$

$$\frac{d^2G}{d\eta^2} = -(\tilde{b} - h^2\cos^2\eta)G(\eta),$$

where k and $\tilde{b}$ are separation constants and $h = ck$. The last equation is the well-known Mathieu equation. The second one is the so called modified or radial Mathieu equation that is obtained from the original one by replacing the real argument by an imaginary one. The solutions of these equations and their stability properties are well documented [9]–[11].

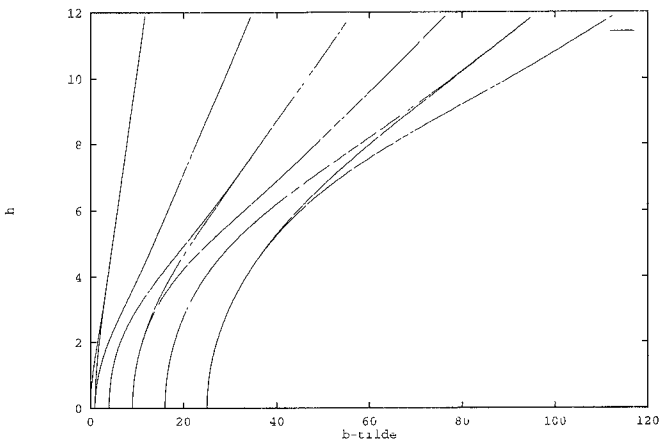

Fig. 2. First several be and bo curves. Parameter $\tilde{b}$ is on the horizontal axis, h is on the vertical one. From left to right the curves are: $be_0, bo_1, be_1, be_2, bo_3, be_4, bo_5, be_5$.

The potential outside and inside the hole for the symmetric case has the form

$$\Phi^s_{\text{out}}(\xi,\eta,z) = (E/2)(|z| - L/2) + \sum_{m=0}^{\infty}\int_0^{\infty} dh \times A_{2m}(h)e^{\frac{-h}{c}(|z|-\frac{L}{2})}\text{Re}_{2m}(h,\xi,\eta),$$

$$\Phi^s_{\text{in}}(\xi,\eta,z) = \sum_{m=0}^{\infty}\sum_{n=1}^{\infty} D_{2m,n}\text{Re}_{2m,n}(h_{2m,n},\xi,\eta) \times \frac{\cosh(h_{2m,n}z/c)}{\cosh(h_{2m,n}L/2c)}. \quad (2.8)$$

We use here the notation $\text{Re}_{2m}(h,\xi,\eta) = \text{Se}_{2m}(h,\eta)\,\text{Je}_{2m}(h,\xi)$. Here Se is the solution of (2.7c), Je is the solution of (2.7b) (see Appendix), and $\text{Re}_{2m,n}$ is $\text{Re}_{2m}(h = h_n)$, where $h_n, n = 1,2,3,\ldots$ is a collection of points on the curves $\text{be}_{2m}, m = 0,1,2,\ldots$, for which $\text{Je}_{2m}(h_n,\xi_0,\eta) = 0$, ξ_0 is the value of ξ at the wall, and $A_{2m}(h)$ and $D_{2m,n}$ are to be found. We now use the matching conditions that the potentials and their first derivatives are equal at $z = \pm L/2$. This gives us the following two equations:

$$\sum_{m=0}^{\infty}\int_0^{\infty} dh A_{2m}\text{Re}_{2m} = \begin{cases}\sum_{m,n} D_{2m,n}\text{Re}_{2m,n} & \text{if } \xi \le \xi_0 \\ 0 & \text{if } \xi > \xi_0\end{cases} \quad (2.9\text{ a,b})$$

$$E/2 - \sum_{m=0}^{\infty}\int_0^{\infty} dh\frac{h}{c}A_{2m}\text{Re}_{2m} = \sum_{m,n} D_{2m,n}\text{Re}_{2m,n}\frac{h_{2m,n}}{c}\tanh(h_{2m,n}L/2c).$$

The simplest way to handle these two equations is to first express A's in terms of D's from (2.9a) and to put the result for A's back into (2.9b). We therefore multiply (2.9a) by $(\cosh^2\xi - \cos^2\eta)\text{Re}_{2p}(h',\xi,\eta)$ and integrate in the interval from 0 to ∞ in ξ and from 0 to 2π in η. After using (A.13c) we get:

$$A_{2m}(h) = \frac{2h}{\pi N_{2m}(h)}\sum_{p,q} D_{2p,q}I_{(2p,q)(2m)}(h),$$

$$I_{(2p,q)(2m)}(h) \equiv \int_0^{\xi_0}\int_0^{2\pi} d\xi d\eta(\cosh^2\xi - \cos^2\eta) \times \text{Re}_{(2p,q)(2m)}(\xi,\eta)\text{Re}_{2m}(h,\xi,\eta).$$

This expression for A is substituted in (2.9b) and the whole equation is multiplied by $(\cosh^2\xi - \cos^2\eta)\text{Re}_{2p,q}$ and integrated from 0 to ξ_0 in ξ and from 0 to 2π in η. After again using (A.13), one obtains:

$$\sum_{r=0}^{\infty}\sum_{s=1}^{\infty}\left\{Q_{(2p.q)(2r,s)} + \frac{\pi}{2}h_{2p,q}\tanh\left(h_{2p,q}\frac{L}{2c}\right) M_{2p,q}\delta_{pr}\delta_{qs}\right\}D_{2r,s} = \frac{\pi cE}{4}T_{2p,q}, \quad (2.10)$$

where

$$Q_{(2p,q)(2r,s)} \equiv \sum_{m=0}^{\infty}\int_0^{\infty} dh\frac{h^2}{N_{2m}(h)} \times I_{(2p,q)(2m)}(h)I_{(2r,s)(2m)}(h),$$

$$T_{2p,q} \equiv \int_0^{\xi_0}\int_0^{2\pi} d\xi d\eta(\cosh^2\xi - \cos^2\eta)\text{Re}_{2p,q},$$

and $M_{2p,q}$ is defined in (A.13). Equation 2.10 is a matrix equation in the D's. Numerical analysis shows that it is enough to keep only three curves—$\text{be}_0, \text{be}_2, \text{be}_4$ ($r = 0,1,2$) on which the quantities Q, M and T are to be calculated, and to take 30 points on each curve ($s = 1,2,\ldots,30$).

Asymptotic expression (see Appendix) tells us that Q, M and T have simple exponential factors that can be taken out:

$$T_{2p,q} = e^{h_{2p,q}}\bar{T}_{2p,q},$$
$$M_{2p,q} = e^{2h_{2p,q}}\bar{M}_{2p,q}, \quad (2.11)$$
$$Q_{(2p,q)(2r,s)} = e^{h_{2p,q}+h_{2r\,s}}\bar{Q}_{(2p,q)(2r,s)}.$$

Solving matrix equation 2.10 completely specifies the symmetric part of the potential both inside and outside the hole. In order to quantify our results, we calculate the electric polarizability:

$$\chi_s \equiv \frac{2}{E}\int_{\text{hole}} dxdy\Phi_s(x,y,z = L/2) = \frac{2c^2}{E}\sum_{m=0}^{\infty}\sum_{n=1}^{\infty} D_{2m,n}T_{2m,n}. \quad (2.12)$$

If we introduce the notation:

$$Z^s_{(2p,q)(2r,s)} \equiv \bar{Q}_{(2p,q)(2r,s)} + \frac{\pi}{2}h_{2p,q}\tanh\left(h_{2p,q}\frac{L}{2c}\right) \times \bar{M}_{2p,q}\delta_{pr}\delta_{qs},$$

combining with (2.11), we get

$$\sum_{r,s} Z^s_{(2p,q)(2r,s)}(e^{h_{2r,s}}D_{2r,s}) = \frac{\pi cE}{4}\bar{T}_{2p,q}.$$

TABLE I
$f_{\text{in}} \equiv \frac{3\chi_{\text{in}}}{2\pi ab^2}$ VERSUS L/b

L/b	$p = 2.48\ 10^{-3}$	$p = 0.2$	$p = 0.4$	$p = 0.6$	$p = 0.8$	$p = 1.0$
0	0.6382	0.7563	0.8567	0.9326	0.9818	1.000
0.01	0.6274	0.7452	0.8454	0.9211	0.9696	0.9884
0.02	0.6193	0.7363	0.8358	0.9110	0.9592	0.9778
0.1	0.5856	0.6946	0.7872	0.8572	0.9020	0.9194
0.2	0.5678	0.6701	0.7570	0.8228	0.8648	0.8811
1.0	0.5476	0.6348	0.7089	0.7649	0.8008	0.8147
2.0	0.5473	0.6329	0.7057	0.7608	0.7960	0.8097
∞	0.5473	0.6329	0.7057	0.7608	0.7960	0.8097

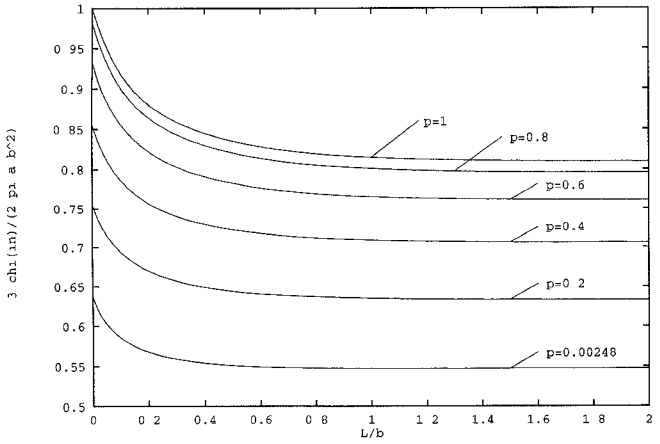

Fig. 3. $f_{in} \equiv \frac{3\chi_{in}}{2\pi ab^2}$ versus L/b. Uppermost curve has the value of $p = 1.0$,; the lowest one is for $p = 2.48 \times 10^{-3}$.

Therefore, the final expression for the polarizability is:

$$\chi_s = \frac{\pi c^3}{2} \sum_{(p,r)(q,s)} \bar{T}_{2p,q} (Z_s^{-1})_{(2p,q)(2r,s)} \bar{T}_{2r,s}. \tag{2.13}$$

For the antisymmetric case we have:

$$\begin{aligned}\Phi^a_{\text{out}}(\xi,\eta,z) &= \pm(E/2)(|z| - L/2) \pm \sum_{m=0}^{\infty} \int_0^{\infty} dh \\ &\quad \times \tilde{A}_{2m}(h) e^{-\frac{h}{c}(|z|-\frac{L}{2})} \mathrm{Re}_{2m}(h,\xi,\eta), \\ \Phi^a_{\text{in}}(\xi,\eta,z) &= \sum_{m=0}^{\infty} \sum_{n=1}^{\infty} \tilde{D}_{2m,n} \mathrm{Re}_{2m,n}(h_{2m,n},\xi,\eta) \\ &\quad \times \frac{\sinh(h_{2m,n} z/c)}{\sinh(h_{2m,n} L/2c)},\end{aligned} \tag{2.14}$$

where $+$ is for $z > L/2$ and $-$ for $z < -L/2$. This gives us the result

$$\chi_a = \frac{\pi c^3}{2} \sum_{(p,r)(q,s)} \bar{T}_{2p,q} (Z_a^{-1})_{(2p,q)(2r,s)} \bar{T}_{2r,s}, \tag{2.15}$$

$$\begin{aligned}Z^a_{(2p,q)(2r,s)} &\equiv \bar{Q}_{(2p,q)(2r,s)} + \frac{\pi}{2} h_{2p,q} \\ &\quad \times \tanh^{-1}\left(h_{2p,q}\frac{L}{2c}\right) \bar{M}_{2p,q} \delta_{pr} \delta_{qs},\end{aligned}$$

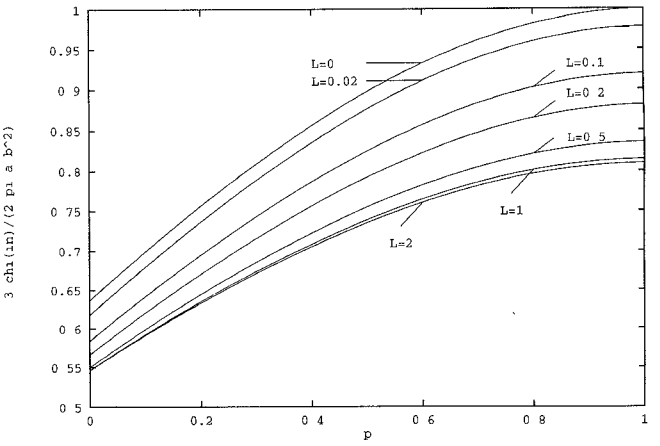

Fig. 4. $f_{in} \equiv \frac{3\chi_{in}}{2\pi ab^2}$ versus p. Uppermost curve has the value of $L = 0.0$, followed by the curves with the parameter $L = 0.02, 0.1, 0.2, 0.5, 1.0$, and 2.0.

In order to simplify the matrix Z one calculates

$$\begin{aligned}I_{(2p,q)(2m)}(h) &= \frac{1}{h^2 - h^2_{2p,q}} K_{(2p,q)(2m)}(h) \\ &\quad \times \left[\mathrm{Je}_{2m} \frac{d\mathrm{Je}_{2p,q}}{d\xi}\right]\Big|_{\xi_0},\end{aligned}$$

with K defined as:

$$K_{(2p,q)(2m)}(h_{2p,q}, h) \equiv \int_0^{2\pi} d\eta \mathrm{Se}_{2p,q}(h_{2p,q},\eta) \mathrm{Se}_{2m}(h,\eta).$$

The properties of the quantity K are discussed in the Appendix.

The calculations are done for different shapes of the elliptical hole. A convenient parameter is $p = (a-b)/(a+b)$. Inside and outside polarizabilities are $\chi_{\text{in}} = \chi_s + \chi_a$ and $\chi_{\text{out}} = \chi_s - \chi_a$. The circular case corresponds to $p = 0$ ($\xi_0 \to \infty$). We have analysed five cases: $p = 0.00248$ ($\xi_0 = 3.$), $p = 0.2, 0.4, 0.6$, and 0.8. For the values of $p > 0.8$, it is difficult to obtain good results using the asymptotic expansion for the Mathieu function. Such cases should be done purely numerically (by the Jacobi relaxation method, for example). The case $p = 1$ is done by Schwarz-Christoffel method and is explained in the next section. In order to compare the results for different cases we keep the area of the ellipses constant ($ab = \text{const} = 1$) and change the thickness of the wall L. For $L = 0$, results are known (see, for example [7]) and we get three significant figures of accuracy. For zero thickness, the result is

$$\frac{1}{\chi} = \frac{3}{2\pi ab^2} E(m),$$

where

$$m = 1 - \frac{b^2}{a^2}, \quad E(m) = \int_0^{\frac{\pi}{2}} d\eta \sqrt{1 - m\sin^2\eta}.$$

On Fig. 3. and in Table I, we display results for $f_{\text{in}} = 3\chi_{\text{in}}/(2\pi ab^2)$ versus L/b. Fig. 4. shows the same quantity versus p. Fig. 5. and Table II show $\log(\chi_{\text{out}}/\chi_0)$ versus L/b, where χ_0 is the value of χ at $L = 0$.

TABLE II
$\log(\chi_{out}/\chi_0)$ VERSUS L/b.

L/b	$p = 2.48\ 10^{-3}$	$p = 0.2$	$p = 0.4$	$p = 0.6$	$p = 0.8$	$p = 1.0$
0	0.000	0.000	0.000	0.000	0.000	0.000
0.01	$-3.661\ 10^{-2}$	$-3.624\ 10^{-2}$	$-3.424\ 10^{-2}$	$-2.866\ 10^{-2}$	$-2.816\ 10^{-2}$	$-2.794\ 10^{-2}$
0.02	$-7.120\ 10^{-2}$	$-6.182\ 10^{-2}$	$-6.071\ 10^{-2}$	$-5.904\ 10^{-2}$	$-5.804\ 10^{-2}$	$-5.268\ 10^{-2}$
0.1	$-3.208\ 10^{-1}$	$-2.681\ 10^{-1}$	$-2.556\ 10^{-1}$	$-2.456\ 10^{-1}$	$-2.400\ 10^{-1}$	$-2.167\ 10^{-1}$
0.2	$-5.973\ 10^{-1}$	$-5.081\ 10^{-1}$	$-4.768\ 10^{-1}$	$-4.521\ 10^{-1}$	$-4.455\ 10^{-1}$	$-3.987\ 10^{-1}$
1.0	$-2.582\ 10^{+0}$	$-2.218\ 10^{+0}$	$-2.040\ 10^{+0}$	$-1.932\ 10^{+0}$	$-1.859\ 10^{+0}$	$-1.699\ 10^{+0}$
2.0	$-4.985\ 10^{+0}$	$-4.267\ 10^{+0}$	$-3.897\ 10^{+0}$	$-3.693\ 10^{+0}$	$-3.533\ 10^{+0}$	$-3.283\ 10^{+0}$

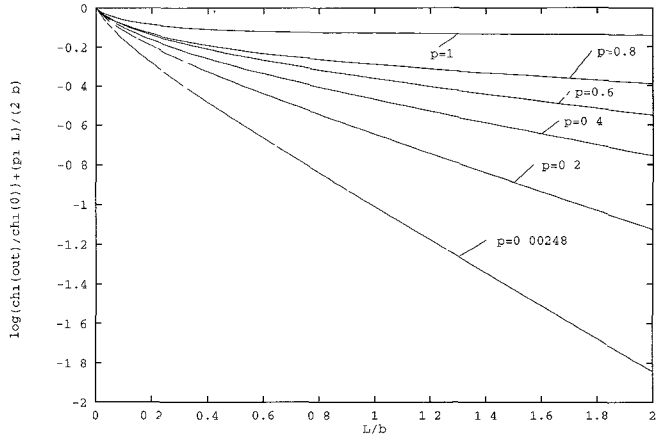

Fig. 5. $log\left(\frac{\chi_{out}}{\chi_0}\right) + \frac{\pi}{2}\frac{L}{b}$ versus L/b The uppermost curve has the value of $p = 1.0$; the lowest one is for $p = 2.48 \times 10^{-3}$.

TABLE III
$f_x \equiv \frac{3\psi_{xx}}{2\pi a^3}$ VERSUS L/a

L/a	$p = 2.48\ 10^{-3}$	$p = 0.2$	$p = 0.4$	$p = 0.6$	$p = 0.8$
0	1.269	0.9546	0.7233	0.5423	0.3840
0.01	1.240	0.9333	0.7043	0.5249	0.3637
0.02	1.217	0.9147	0.6877	0.5086	0.3462
0.1	1.106	0.8155	0.5975	0.4226	0.2597
0.2	1.031	0.7477	0.5353	0.3641	0.2081
1.0	0.9055	0.6346	0.4320	0.2702	0.1360
2.0	0.8995	0.6294	0.4274	0.2662	0.1332
∞	0.8995	0.6294	0.4274	0.2662	0.1332

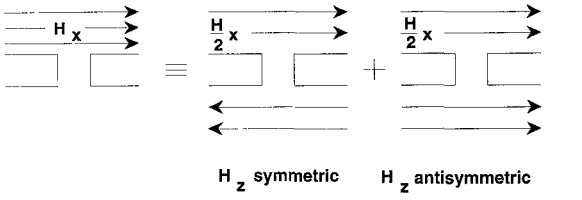

Fig. 6. Separation of magnetic fields in both directions into symmetric and antisymmetric components.

B. Magnetic Case

We decompose the magnetic case too into the symmetric and antisymmetric part as in Fig. 6., and we treat separately two situations $H_x \neq 0, H_y = 0$ and $H_x = 0, H_y \neq 0$. For the case $H_x \neq 0$, we need a solution that should be even when $\eta \to -\eta$ and odd when $\eta \to \pi - \eta$. When $H_y \neq 0, H_x = 0$ the symmetry is opposite. That allows us to write the solution for the potential in the form

$$\Psi^{s,x}_{\text{out}}(\xi,\eta,z) = -xH_x/2 + \sum_{m=0}^{\infty}\int_0^{\infty} dh A^x_{2m+1}(h) \times e^{-\frac{h}{c}\left(|z|-\frac{L}{2}\right)}\text{Re}_{2m+1}(h,\xi,\eta),$$

$$\Psi^{s,x}_{\text{in}}(\xi,\eta,z) = \sum_{m=0}^{\infty}\sum_{n=1}^{\infty} D^x_{2m+1,n}\text{Re}_{2m+1,n} \times (h_{2m+1,n},\xi,\eta)\frac{\sinh(h_{2m+1,n}z/c)}{\sinh(h_{2m+1,n}L/2c)}. \quad (2.16)$$

$$\Psi^{s,y}_{\text{out}}(\xi,\eta,z) = -yH_y/2 + \sum_{m=0}^{\infty}\int_0^{\infty} dh \times A^y_{2m+1}(h)e^{-\frac{h}{c}\left(|z|-\frac{L}{2}\right)}\text{Ro}_{2m+1}(h,\xi,\eta),$$

$$\Psi^{s,y}_{\text{in}}(\xi,\eta,z) = \sum_{m=0}^{\infty}\sum_{n=1}^{\infty} D^y_{2m+1,n}\text{Ro}_{2m+1,n} \times (h_{2m+1,n},\xi,\eta)\frac{\sinh(h_{2m+1,n}z/c)}{\sinh(h_{2m+1,n}L/2c)}. \quad (2.17)$$

Here, we have $\text{Ro}_{2m+1} = \text{Jo}_{2m+1}(h,\xi)\text{So}_{2m+1}(h,\eta)$ and $h_{2m+1,n}$, $m = 0,1,2,\ldots, n = 1,2,3,\ldots$ is a set of points on the curves $\text{be}_{2m+1}, \text{bo}_{2m+1}$ where $\frac{\partial \text{Je,o}_{2m+1}(h_{2m+1,n},\xi)}{\partial\xi}|_{\xi_0} = 0$ in the H_x and H_y cases respectively. In the antisymmetric case, $\sinh(\alpha)$ will be replaced by $\cosh(\alpha), \alpha = h_{2m+1,n}z/c$ or $\alpha = h_{2m+1,n}L/2c$. These two sets of equations are treated separately and in the same way as in the electric case. With the help of (A.13) one calculates:

$$\sum_{r,s} Z^{s,x,y}_{(2p+1,q)(2r+1,s)}\left(e^{h_{2r+1,s}}V^{x,y}_{2r+1,s}\right) = -cH_{x,y}\bar{T}^{x,y}_{2p+1,q}, \quad (2.18)$$

with the following definitions:

$$Z^{s,v,y}_{(2p+1,q)(2r+1,s)} \equiv \bar{Q}_{(2p+1,q)(2r+1,s)} + \frac{\pi}{2}h^{-1}_{2p+1,q} \times \tanh(h_{2p+1,q}L/2c)\bar{M}^{x,y}_{2p+1,q}\delta_{pr}\delta_{qs},$$

$$V^{x,y}_{2r+1,s} \equiv \frac{2}{\pi}h_{2r+1,s}\tanh^{-1}(h_{2r+1,s}L/2c)D^{x,y}_{2r+1,s},$$

$$Q_{(2p+1,q)(2r+1,s)} \equiv \sum_{m=0}^{\infty}\int_0^{\infty} dh \frac{1}{N_{2m+1}(h)} \times I_{(2p+1,q)(2m+1)}(h)I_{(2r+1,s)(2m+1)}(h),$$

TABLE IV
$\log(\psi_{xx,\mathrm{out}}/\psi_{xx,0})$ VERSUS L/a

L/a	$p = 2.48\ 10^{-3}$	$p = 0.2$	$p = 0.4$	$p = 0.6$	$p = 0.8$
0	0.000	0.000	0.000	0.000	0.000
0.01	$-2.783\ 10^{-2}$	$-2.805\ 10^{-2}$	$-2.833\ 10^{-2}$	$-2.895\ 10^{-2}$	$-6.345\ 10^{-2}$
0.02	$-6.121\ 10^{-2}$	$-6.208\ 10^{-2}$	$-6.557\ 10^{-2}$	$-6.766\ 10^{-2}$	$-1.179\ 10^{-1}$
0.1	$-2.661\ 10^{-1}$	$-2.737\ 10^{-1}$	$-2.913\ 10^{-1}$	$-3.222\ 10^{-1}$	$-4.607\ 10^{-1}$
0.2	$-4.844\ 10^{-1}$	$-5.006\ 10^{-1}$	$-5.303\ 10^{-1}$	$-5.839\ 10^{-1}$	$-7.799\ 10^{-1}$
1.0	$-2.012\ 10^{+0}$	$-2.057\ 10^{+0}$	$-2.118\ 10^{+0}$	$-2.219\ 10^{+0}$	$-2.504\ 10^{+0}$
2.0	$-3.857\ 10^{+0}$	$-3.924\ 10^{+0}$	$-4.000\ 10^{+0}$	$-4.109\ 10^{+0}$	$-4.400\ 10^{+0}$

TABLE V
$f_y \equiv \frac{3\psi_{yy}}{2\pi a b^2}$ VERSUS L/b

L	$p = 0$	$p = 0.2$	$p = 0.4$	$p = 0.6$	$p = 0.8$	$p = 1.0$
0	1.273	1.168	1.095	1.044	1.013	1.000
0.01	1.246	1.146	1.078	1.031	1.001	0.9884
0.02	1.225	1.129	1.063	1.018	0.9898	0.9778
0.1	1.108	1.035	0.9848	0.9504	0.9285	0.9194
0.2	1.032	0.9739	0.9336	0.9060	0.8885	0.8811
1.0	0.9099	0.8731	0.8477	0.8303	0.8193	0.8147
2.0	0.9038	0.8675	0.8424	0.8252	0.8143	0.8097
∞	0.9038	0.8675	0.8424	0.8252	0.8143	0.8097

$$T^x_{2p+1,q} \equiv \int_0^{\xi_0}\int_0^{2\pi} d\xi d\eta(\cosh^2\xi - \cos^2\eta) \times \cosh\xi\cos\eta \mathrm{Re}_{2p+1,q},$$

$$T^y_{2p+1,q} \equiv \int_0^{\xi_0}\int_0^{2\pi} d\xi d\eta(\cosh^2\xi - \cos^2\eta) \times \sinh\xi\sin\eta \mathrm{Ro}_{2p+1,q},$$

$$I_{(2p+1,q)(2m+1)}(h) = \frac{1}{h^2 - h^2_{2p,q}} K_{(2p+1,q)(2m+1)}(h) \times \left[\mathrm{Je}_{2p+1,q}\frac{d\mathrm{Je}_{2m+1}}{d\xi}\right]\Big|_{\xi_0}, \quad (2.19)$$

and with (2.11) valid in this case too. The quality M is defined in (A.13) with R being Re and Ro in H_x and H_y case, respectively. Antisymmetric case will have $\tanh(\alpha) \to \tanh^{-1}(\alpha)$ in (2.19a) and (2.19b).

The quantity that we now calculate is the tensor of susceptibility:

$$\psi_{xx}H_x + \psi_{xy}H_y = \int_{\mathrm{hole}} xdxdyH_z(x,y,z = L/2),$$
$$\psi_{yx}H_x + \psi_{yy}H_y = \int_{\mathrm{hole}} ydxdyH_z(x,y,z = L/2) \quad (2.20)$$

This tensor will be diagonal if we choose the axes of the ellipse, so we can write

$$\psi_{xx} = \frac{1}{H_x}\int_{\mathrm{hole}} xdxdyH_z(x,y,z = L/2),$$
$$\psi_{yy} = \frac{1}{H_y}\int_{\mathrm{hole}} ydxdyH_z(x,y,z = L/2) \quad (2.21)$$

where H_z in the upper equation is induced by H_x and in the lower equation is induced by H_y. Using the elliptical

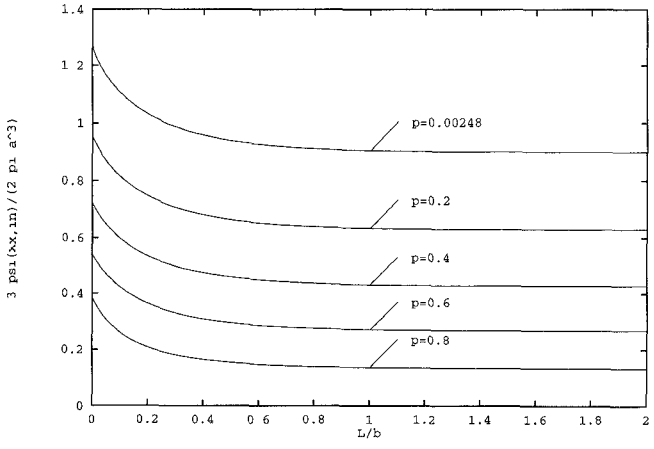

Fig. 7. $f_x \equiv \frac{3\psi_{xx,in}}{2\pi a^3}$ versus L/a. Uppermost curve has the value of $p = 2.48 \times 10^{-3}$; the lowest one is for $p = 0.8$.

coordinates and the induced field $H_z = -\frac{\partial\psi}{\partial z}$ we have

$$\psi_{xx} = -\frac{\pi c^2}{2H_x}\sum_{m,n} V^x_{2m+1,n}T^x_{2m+1,n}$$
$$\psi_{yy} = -\frac{\pi c^2}{2H_y}\sum_{m,n} V^y_{2m+1,n}T^y_{2m+1,n}.$$

Inverting (2.18) we obtain the final form for the susceptibilities

$$\psi^{s,a}_{xx} = \frac{\pi c^3}{2}\sum_{(p,r)(q,s)} \bar{T}^x_{2p+1,q}(Z^{-1}_{s,a})_{(2p+1,q)(2r+1,s)}\bar{T}^x_{2r+1,s},$$
$$\psi^{s,a}_{yy} = \frac{\bar{u}c^3}{2}\sum_{(p,r)(q,s)} \bar{T}^y_{2p+1,q}(Z^{-1}_{s,a})_{(2p+1,q)(2r+1,s)}\bar{T}^y_{2r+1,s}. \quad (2.22)$$

The Z matrix is defined on the be_{2m+1} curves in H_x case and on the bo_{2m+1} curves in H_y case. For zero thickness, we express known results in the form of the standard elliptic integrals

$$\frac{1}{\psi_{xx}} = \frac{3}{2\pi a^3 m}(K(m) - E(m)),$$
$$\frac{1}{\psi_{yy}} = \frac{3}{2\pi a b^2 m}((m-1)K(m) + E(m)),$$
$$m = 1 - \frac{b^2}{a^2}, \quad E(m) = \int_0^{\frac{\pi}{2}} d\eta\sqrt{1 - m\sin^2\eta},$$

TABLE VI
$\log(\psi_{yy,\mathrm{out}}/\psi_{yy,0})$ VERSUS L/b

L/b	$p=0.0$	$p=0.2$	$p=0.4$	$p=0.6$	$p=0.8$	$p=1.0$
0	0.000	0.000	0.000	0.000	0.000	0.000
0.01	$-3.655\ 10^{-2}$	$-3.116\ 10^{-2}$	$-2.806\ 10^{-2}$	$-1.741\ 10^{-2}$	$-1.701\ 10^{-2}$	$-1.699\ 10^{-2}$
0.02	$-6.616\ 10^{-2}$	$-6.037\ 10^{-2}$	$-5.612\ 10^{-2}$	$-4.499\ 10^{-2}$	$-4.413\ 10^{-2}$	$-4.397\ 10^{-2}$
0.1	$-2.710\ 10^{-1}$	$-2.574\ 10^{-1}$	$-2.486\ 10^{-1}$	$-2.349\ 10^{-1}$	$-2.239\ 10^{-1}$	$-2.167\ 10^{-1}$
0.2	$-4.895\ 10^{-1}$	$-4.715\ 10^{-1}$	$-4.595\ 10^{-1}$	$-4.499\ 10^{-1}$	$-4.320\ 10^{-1}$	$-3.986\ 10^{-1}$
1.0	$-2.014\ 10^{+0}$	$-1.975\ 10^{+0}$	$-1.942\ 10^{+0}$	$-1.893\ 10^{+0}$	$-1.825\ 10^{+0}$	$-1.699\ 10^{+0}$
2.0	$-3.856\ 10^{+0}$	$-3.784\ 10^{+0}$	$-3.711\ 10^{+0}$	$-3.636\ 10^{+0}$	$-3.512\ 10^{+0}$	$-3.283\ 10^{+0}$

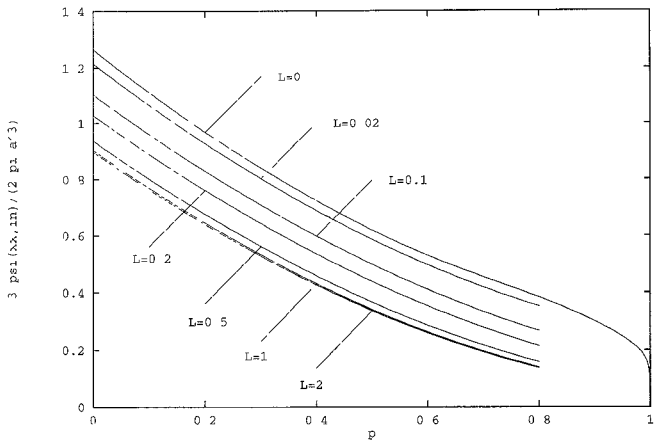

Fig. 8. $f_x \equiv \frac{3\psi_{xx,in}}{2\pi a^3}$ versus p. Uppermost curve has the value of $L. = 0.0$, followed by the curves with the parameters $L = 0.02, 0.1, 0.2, 0.5, 1.0$, and 2.0. Exact results are known for $L = 0.0$ curve; it has the value 0.0 for $p = 1$.

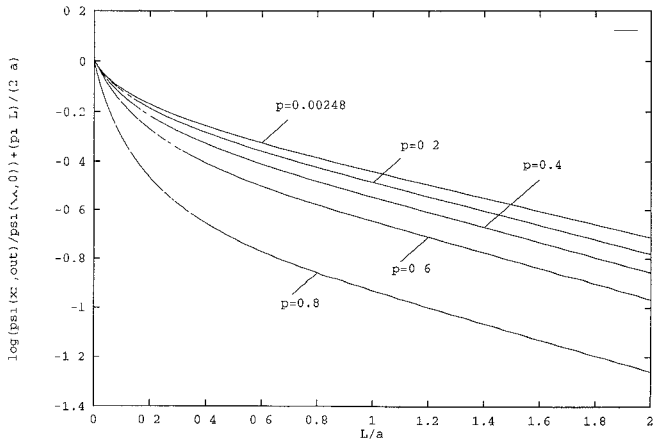

Fig. 9. $log\left(\frac{\psi_{xx,\mathrm{out}}}{\psi_{xx,0}}\right) + \frac{\pi}{2}\frac{L}{a}$. The uppermost curve has the value of $p = 2.48 \times 10^{-3}$, the lowest is for $p = 0.8$.

$$K(m) = \int_0^{\frac{\pi}{2}} d\eta \frac{1}{\sqrt{1 - m\sin^2\eta}}.$$

We find it convenient to define $f_x = 3\psi_{xx}/(2\pi a^3)$, $f_y = 3\psi_{yy}/(2\pi ab^2)$, where the susceptibilities are calculated inside the hole. These quantities are drawn in Figs. 7 and 10 for different values of p versus L/a for the x case and L/b for the y case. The normalized susceptibilities outside the hole for different values of p are shown in Figs. 9 and 12. Tables III–VI contain that information in numerical form.

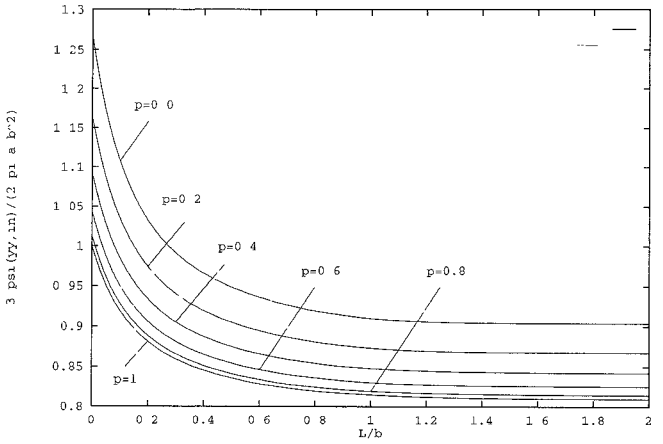

Fig. 10. $f_y \equiv \frac{3\psi_{yy,in}}{2\pi ab^2}$ versus L/b. Uppermost curve has the value of $p = 0.0$; the lowest one is for $p = 1.0$.

III. INFINITELY LONG ELLIPTICAL HOLE

This case corresponds to $b/a \to 0$, i.e. $p = 1$, and can be treated as 2-dimensional case (see Fig. 13). The Schwarz-Christoffel transformation is used: the polygon (1, 2, 3, 4, 5) in Fig. 13 in the original geometry is transformed into the upper half of the w-plane by the transformation

$$dz = dw(w+P)^{-\frac{1}{2}} w^{-\frac{1}{2}} (w-Q)^{\frac{1}{2}}, \tag{3.1}$$

where P and Q are real and positive and are found from the width of the hole b and the thickness of the wall L:

$$b = \int_0^{z_3} dz = \int_{-P}^{0} dw(w+P)^{-\frac{1}{2}} w^{-\frac{1}{2}} (w-Q)^{\frac{1}{2}} = 2\sqrt{P+Q}E(m), \tag{3.2}$$

where $m = P/(P+Q)$. We also have

$$i\frac{L}{2} = \int_{z_3}^{z_4} dz = 2i\sqrt{P+Q}(K(m_1) - E(m_1)),$$
$$m_1 = 1 - m,$$

so that the combination of the last two formulas will give:

$$\frac{L}{2b} = \frac{K(m_1) - E(m_1)}{E(m)}. \tag{3.3}$$

In order to get the polarizability, we have to integrate the potential along the line orthogonal to the y axis (1, 2 line in

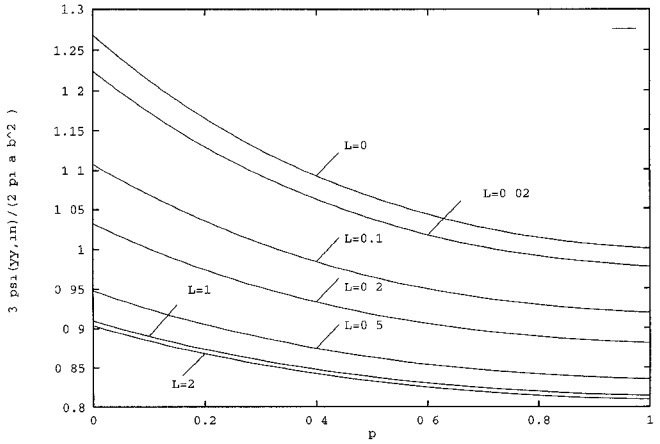

Fig. 11. $f_y \equiv \frac{3\psi_{yy,in}}{2\pi ab^2}$ versus p. Uppermost curve has the vlaue of $L = 0.0$, followed by the curves with the parameters $L = 0.02, 0.1, 0.2, 0.5, 1.0$, and 2.0.

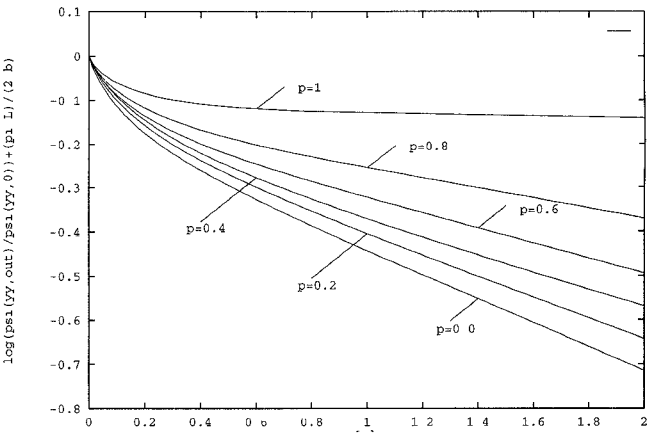

Fig. 12. $\log\left(\frac{\psi_{yy,\text{out}}}{\psi_{yy,0}}\right) + \frac{\pi}{2}\frac{L}{b}$. The lowest curve has the value of $p = 0.0$; the uppermost is for $p = 1.0$.

Fig. 13) in the z-plane and emanating from point 4. Integration is done in the w plane and we get:

$$\frac{x}{b} + i\frac{y}{b} = \frac{E(\theta, m)}{E(m)}, \tag{3.4}$$

where $\theta = \alpha + i\beta$ and $E(\theta, m) = \int_0^\theta d\phi\sqrt{1 - m\sin^2\phi}$.

In the symmetric case the transformation $w = -t^2$ brings the potential to the form $\Phi = (E/2)\mathrm{Re}(t)$. In the antisymmetric case the transformation is $w = t^2$ and the potential becomes $\Phi = (E/2)\mathrm{Im}(v)$. Combining now the formulas 3.2, 3.3, and 3.4, one obtains

$$\Phi_s\left(x, y = \frac{L}{2}\right) = \frac{E}{2}\frac{b\sqrt{m}}{E(m)}\cos\alpha\cosh\beta,$$
$$\Phi_a\left(x, y = \frac{L}{2}\right) = \frac{E}{2}\frac{b\sqrt{m}}{E(m)}\cos\alpha\sinh\beta. \tag{3.5}$$

The real variables α and β are found numerically by inverting (3.4) for $y = L/2$ and $0 < x < b$. This inversion is achieved by the use of Mathematica, which handles special functions with ease. Integrating (3.5) gives the numerical results accurate to four significant figures, as can be confirmed by reducing the integration step in a few sample calculations. They give the values of χ and ψ_y for $p = 1$. Further reduction of the integration step would increase the accuracy, but the time of integration would also increase. The compromise gives the achieved accuracy.

IV. Summary

The penetration of electric and magnetic fields through an elliptical hole in a wall of finite thickness has been investigated. The inside and outside polarizability of the hole are calculated as a function of the parameter $p = (a-b)/(a+b)$ and the relative thickness of the wall (L/a or L/b) and displayed in Figs. 3, 4, and 5.

The inside and outside magnetic susceptibilities of the hole in two perpendicular directions (parallel to the major and minor axes of the ellipse) are calculated and shown in Figs. 7–12. A combination of analytical treatment of the Mathieu

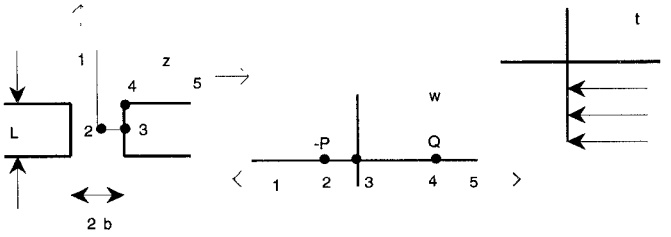

Fig. 13. The Schwarz-Cristoffel transformation maps the polygon (1,2,3,4,5) in the z plane into the upper half of the w plane. The upper half of w plane is then mapped into the t plane in which the potential is homogeneous.

equation and numerical results gives good results for the values of the parameter $p \leq 0.8$. The Schwarz-Cristoffel conformal mapping technique gives the solution to the problem for $p = 1$. By judicious choice of plotted variables, we were able to interpolate smoothly, and thus cover the whole region $0 \leq p \leq 1$ corresponding to all values of eccentricities of the ellipse.

For the magnetic susceptibility in x direction, we know that for any thickness L of the wall the value of ψ_{xx} must be zero when $p = 1$. We were not able to find a simple dependence of ψ_{xx} on p for $0.8 \leq p \leq 1$ when $L \neq 0$.

Our results are in good agreement (four significant figures) with the known results for different limiting cases: 1) when the thickness of the wall goes to zero (analytical results are available), 2) when the ellipse approaches the circle (the results are given in [8]), and 3) when $b/a \to 0$, in which case a two-dimensional problem is obtained and solved by the Schwarz-Cristoffel conformal mapping technique. The analysis of the general case that we present in this paper is based on the properties of the Mathieu equation and differs mutually from any of the three methods used to calculate the three limiting cases.

V. Appendix

In what follows, the basic properties of the solutions of the Mathieu and the modified Mathieu equations are analyzed. Most of the analytic and numerical results we need are assembled in [11], but the numerical results give the properties

of these solutions only for $h < 10$. Asymptotic expression of the solution of the periodic equation is not valid in the whole region $(0, 2\pi)$. Since we need the solutions for h up to 2000, more numerical and analytical work is needed.

A. Characteristic Values

We are looking for the solutions of the Mathieu equation that are periodic with periods π and 2π. The values of $\tilde{b}$ that give such solutions for any given h are called the characteristic values. They, of course, depend on h and comprise curves $\mathrm{be}_m(m = 0, 1, 2, 3, \ldots)$ and $\mathrm{bo}_m(m = 1, 2, 3, \ldots)$ in the $(\tilde{b}, h)$ plane (Fig. 2). From each of the points $m^2(m = 1, 2, \ldots)$, two curves originate (bo_m and be_m), the first one being positioned to the left with respect to the latter one. From the point (0, 0) only one curve originates—be_0. The curves $\mathrm{bo}_m(m = 2, 4, 6, \ldots)$ are not displayed since we do not need them. For small h we use power series expansion [12], for intermediate values ($5 < h < 100$) we use numerical methods, and for large values of h and asymptotic series is given:

$$\tilde{b} = \sum_{i=-1}^{\infty} a_i h^{-i}, \tag{A.1}$$

where the first several terms are: $a_{-1} = \nu$, $a_0 = -\frac{\nu^2+1}{8}$, $a_1 = -\frac{\nu^3+3\nu}{2^6}$, $a_2 = -\frac{5\nu^4+34\nu^2+9}{2^{10}}$, $a_3 = -\frac{33\nu^5+410\nu^3+405\nu}{2^{14}}$, $a_4 = -\frac{63\nu^6+1260\nu^4+2943\nu^2+486}{2^{16}}$, $a_5 = -\frac{527\nu^7+15617\nu^5+69001\nu^3+41607\nu}{2^{20}}$ and $\nu = 2r + 1$ for the function be_r and $\nu = 2r - 1$ for the function bo_r. We achieve high accuracy for these curves (at least 10 significant figures).

B. Solutions

The symmetry conditions require that in the electric case we take only those solutions that are periodic with period π and symmetric with respect to transformation $\eta \to -\eta$. That brings us to the curves be_{2m} $m = 0, 1, 2, \ldots$ where the solution has the form

$$G(\eta) \equiv \mathrm{Se}_{2m}(h, \eta) = \sum_{n=0}^{\infty} \mathrm{Be}_{2n}^{2m}(h) \cos(2n\eta), \quad m = 0, 1, 2, \ldots. \tag{A.2}$$

The normalization condition that we use is

$$G(\eta = 0) = 1 \Rightarrow \sum_{n=0}^{\infty} \mathrm{Be}_{2n}^{2m}(h) = 1. \tag{A.3}$$

Inserting the Fourier series (A.2) into the differential equation (2.7c), one derives ($\mathrm{Be}_{2n}^{2m} B_{2n}$):

$$\begin{aligned} B_2 &= k_0 B_0, \\ B_4 &= k_2 B_2 - 2B_0, \\ K_{2n} B_{2n} &= B_{2n+2} + B_{2n-2} \\ k_m &= h^{-2}(4b - 2h^2 - 4m^2). \end{aligned} \tag{A.4}$$

If one defines $G_m = B_m / B_{m-2}$, $m = 2, 4, \ldots$ one has:

$$G_2 = k_0, \quad G_4 = k_2 - 2/k_0, \quad G_{2n} = k_{2n-2} - \cfrac{1}{k_{2n-4} - \cfrac{1}{k_{2n-6} - \cdots}} \qquad n > 2, \tag{A.5}$$

which together with (A.3) gives us the values for $\mathrm{Be}_{2n}^{2m}(h)$. Since in (A.5) we have to divide by terms that can be zero, we use relational approximation for treating continued fractions [8], which gives us results accurate to at least 10 significant figures, but only for $h < H_{cr} \equiv 20.00$. This is because Be_{2n}^{2m} alternate in signs, grow exponentially, but have to satisfy A.3, so for $h \approx 50$ one would have to know B's with the accuracy of 22 significant figures in order to satisfy (A.3) to two significant figures. This forces us to use asymptotic expression for values of $h > 20$.

The solution for two different magnetic cases will be of the form:

$$\begin{aligned} H_x \neq 0, \quad H_y = 0 \Rightarrow G(\eta) &\equiv \mathrm{Se}_{2m+1}(h, \eta) \\ &= \sum_{n=0}^{\infty} \mathrm{Be}_{2n+1}^{2m+1}(h) \cos[(2n+1)\eta], \\ H_x = 0, \quad H_y \neq 0 \Rightarrow G(\eta) &\equiv \mathrm{So}_{2m+1}(h, \eta) \\ &= \sum_{n=0}^{\infty} \mathrm{Bo}_{2n+1}^{2m+1}(h) \sin[(2n+1)\eta]. \end{aligned} \tag{A.6}$$

This is so because we want the solution to be even for $\eta \to -\eta$ and odd for $\eta \to \pi - \eta$ when $H_x \neq 0$ and to have opposite symmetry when $H_y \neq 0$. The relevant formulas for $\mathrm{Be}_{2n+1}^{2m+1}(h)$ and $\mathrm{Bo}_{2n+1}^{2m+1}(h)$ are derived in an analogous way to those in (A.2)–(A.4). The solutions for the modified (radial) Mathieu (2.7b) are given as:

$$\begin{aligned} F(\xi) &\equiv \mathrm{Je}_{2r+p}(h, \xi) \\ &= \sqrt{\pi/2}(-1)^r \sum_{k=0}^{\infty} (-1)^k \mathrm{Be}_{2k+p}^{2r+p}(h) J_{2k+p}(h \cosh \xi), \\ F(\xi) &\equiv \mathrm{Jo}_{2r+p}(h, \xi) \\ &= \sqrt{\pi/2}(-1)^r \tanh(\xi) \sum_{k=0}^{\infty} (-1)^k (2k+p) \\ &\quad \times \mathrm{Bo}_{2k+p}^{2r+p}(h) J_{2k+p}(h \cosh \xi), \end{aligned} \tag{A.7}$$

where $r = 0, 1, 2, \ldots$, $p = 0, 1$, Je_m is defined on $\mathrm{be}_m(h)$, Jo_m is defined on $\mathrm{bo}_m(h)$ and J's are the Bessel functions. The normalization in these solutions is chosen in such a way to give simple asymptotic expansion when $\xi \to \infty$:

$$\begin{aligned} \mathrm{Je}_m(h, \xi) &\cong \mathrm{Jo}_m(h, \xi) \\ &\cong \cos[h \cosh \xi - (2m+1)\pi/4] / \sqrt{h \cosh \xi}. \end{aligned}$$

Unfortunately, numerical analysis shows that this simple asymptotic expansion is good only for moderate values of h—when (A.7) converges rapidly enough. The other solution to (2.7b) blows up at the origin and is not of interest.

C. Asymptotic Expressions Elementary numerical analysis shows that the solution for the Mathieu equation has exponential behavior for large values of h. Since the solution for the radial equation is related to the solution of the Mathieu equation by the replacement of a real argument by a purely imaginary one, one can look for the solution of the radial equation in the following form [11]:

$$F(\xi) = e^{ih\phi_0(\xi)} \psi(\xi) \left[1 + \frac{\phi_1(\xi)}{h} + \frac{\phi_2(\xi)}{h^2} + \cdots \right],$$

Substituting this expansion into 2.7b and using A.1 one arrives at:

$$\begin{aligned}\mathrm{Je}_r &\cong [F_0(\xi)\cos\alpha + F_1(\xi)\sin\alpha]\sqrt{h\cosh\xi},\\ \mathrm{Jo}_{r+1} &\cong [F_0(\xi)\sin\alpha - F_1(\xi)\cos\alpha]\sqrt{h\cosh\xi},\end{aligned} \quad \text{(A.8)}$$

where $\alpha = h\sinh\xi - (2r+1)\arctan(\tanh(\xi/2))$, $\nu = 2r+1$, and

$$\begin{aligned}F_0(\xi) &= 1 + \frac{\nu}{4h\cosh^2\xi}\\ &\quad + \frac{1}{h^2}\left[\frac{\nu^4+86\nu^2+105}{512\cosh^4\xi} - \frac{\nu^4+22\nu^2+57}{512\cosh^2\xi}\right]\\ &\quad + \frac{1}{h^3}\left[\frac{3\nu^5+290\nu^3+1627\nu}{2048\cosh^6\xi}\right.\\ &\quad - \frac{2\nu^5+124\nu^3+1122\nu}{2048\cosh^4\xi}\\ &\quad \left. - \frac{\nu^5+14\nu^3+33\nu}{2048\cosh^2\xi}\right] + \cdots,\\ F_1(\xi) &= \frac{(\nu^3+3)\sinh\xi}{16h\cosh^2\xi}\\ &\quad + \frac{\sinh\xi}{128h^2\cosh^2\xi}\left[\nu^3+3\nu+\frac{4\nu^3+44\nu}{\cosh^2\xi}\right]\\ &\quad + \frac{\sin h\xi}{h^3}\left[\frac{\nu^6+505\nu^4+12139\nu^2+10395}{24576\cosh^6\xi}\right.\\ &\quad - \frac{\nu^6-47\nu^4+667\nu^2+2835}{24576\cosh^4\xi}\\ &\quad \left. + \frac{5\nu^4+34\nu^2+9}{2048\cosh^2\xi}\right] + \cdots\end{aligned}$$

This expansion easily gives us six significant figures accuracy for any $h > H_{cr}$. The same procedure will gives us the expansion for Se and So solutions of the Mathieu equation:

$$\begin{aligned}\mathrm{Se}_r(h,\eta) &\cong \sigma_r\{W_1[P_0(\eta) - P_1(\eta)]\\ &\quad + W_2[P_0(\eta) + P_1(\eta)]\},\\ \mathrm{So}_{r+1}(h,\eta) &\cong \tau_{r+1}\{W_1[P_0(\eta) - P_1(\eta)]\\ &\quad - W_2[P_0(\eta) + P_1(\eta)]\},\end{aligned} \quad \text{(A.9)}$$

where $\nu = 2r+1$ and

$$\begin{aligned}W_1(\eta) &= e^{h\sin\eta}\left[\cos\left(\frac{\eta}{2}+\frac{\pi}{4}\right)\right]^{2r+1}\Big/(\cos\eta)^{r+1},\\ W_2(\eta) &= e^{-h\sin\eta}\left[\sin\left(\frac{\eta}{2}+\frac{\pi}{4}\right)\right]^{2r+1}\Big/(\cos\eta)^{r+1}.\\ \sigma_r(h) &= 2^{r-\frac{1}{2}}\left[1+\frac{\nu}{4h}+\frac{4\nu^2+3}{32h^2}+\frac{19\nu^3+59\nu}{256h^3}+\cdots\right]^{-1},\\ \tau_{r+1}(h) &= 2^{r-\frac{1}{2}}\left[h-\nu/4-\frac{2\nu^2+3}{32h}-\frac{7\nu^3+47\nu}{256h^2}-\cdots\right]^{-1},\end{aligned}$$

and where $P_0(\eta)$ and $P_1(\eta)$ are obtained from $F_0(\xi)$ and $F_1(\xi)$ by substitution $\cosh\xi \to \cos\eta$ and $\sinh\xi \to \sin\eta$. Since in the process of deriving (A.9) we had to divide by $\cos\eta$, it comes to no surprise that (A.9) is divergent at $\pi/2$. Taylor series expansion is used in the region around $\pi/2$ and matched with the formulas A.9. Here comes the first serious problem: At what point between 0 and $\pi/2$ do we match A.9 and the Taylor expansion? Numerical analysis shows that that point depends strongly on r and on h. We are at this point tempted to find another asymptotic expansion for the solution of (2.3c)—WKB expansion.

The solution of the equation $\frac{d^2G(\eta}{d\eta^2)} - \lambda Q(\eta)G(\eta) = 0$ for λ large can easily be expanded into series in $1/\lambda$. But the Mathieu equation gives us two problems here: $Q(\eta) = (\tilde{b} - \cos^2\eta)$ has second-order zero $\pi/2$, thus giving the solution in terms of the confluent hypergeometric function of the third kind (Whittaker functions) [14], which are difficult to handle when we impose boundary conditions (A.3), and worse, $\tilde{b}$ depends on h, which has the effect that the independent expansion variable in the Whittaker function also depends on h. Numerical trials show that for h we are interested in that series does not converge.

That sends us back to A.9. We find numerically that the point $\rho(h)$ between 0 and $\pi/2$ at which matching is done depends on h in a simple way: $\rho(h) = \sum_{i=0}^{\infty} g_i h^{-i}$, where only several terms are needed and where constants g_i depend on which curve be_r, bo_r we are on. Twenty terms in the Taylor expansion and 5 terms in ρ give us 4 to 5 significant figures for any h.

We now look in some details at the following constructs:

$$\begin{aligned}N_{2m}(h) &= \int_0^{2\pi} d\eta[\mathrm{Se}_{2m}(h,\eta)]^2\\ &= \pi[2B_0^2 + B_2^2 + B_4^2 + \cdots],\\ N^e_{2m+1}(h) &= \int_0^{2\pi} d\eta[\mathrm{Se}_{2m+1}(h,\eta)]^2\\ &= \pi[B_1^2 + B_3^2 + B_5^2 + \cdots],\\ N^o_{2m+1}(h) &= \int_0^{2\pi} d\eta[\mathrm{So}_{2m+1}(h,\eta)]^2\\ &= \pi[B_1^2 + B_3^2 + B_5^2 + \cdots].\end{aligned} \quad \text{(A.10)}$$

The right hand sides are numerically valid for $h < H_{cr} = 20$. For higher values of h expansion A.9 is used together with the Laplace method for the asymptotic evaluation of integrals (see, for example [15]). It follows that

$$N_m^{e,o} = \frac{1}{h^m}\sqrt{\frac{\pi}{h}}e^{2h}\bar{N}_m^{e,o}(h), \quad m = 0,1,2,\ldots, \quad \text{(A.11)}$$

where $\bar{N}_m^{e,o} = \sum_{i=0}^{\infty} a_i h^{-i}$ and only several terms are needed to achieve desired accuracy.

Next we take the cross product

$$\begin{aligned}K^{e,o}_{(2p+r,q)(2m+r)}(h_q,h) &= \int_0^{2\pi} G_{2p+r,q}(h_q,\eta)G_{2m+r}(h,\eta),\\ &\quad r = 0,1, \quad p,m = 0,1,2,\ldots,\end{aligned}$$

where $G = \mathrm{Se}, \mathrm{So}$ and h_q is a certain fixed value of h on the corresponding curve be or bo. If both G's are evaluated on the same curve ($m = p$) $K \neq 0$ for $h_q = h$ and $K = 0$ for $h_q = h$ if $m \neq p$. Using (A.9) and the Laplace method, we obtain:

$$\begin{aligned}&K^{e,o}_{(2p+r,q)(2m+r)}(h_q,h)\\ &\quad = \frac{1}{\bar{h}^{m+p+r}}\sqrt{\frac{\pi}{\bar{h}}}e^{2\bar{h}}(h-h_q)^s\bar{K}^{e,o}_{(2p+r,q)(2m+r)}(h_q,h),\end{aligned} \quad \text{(A.12)}$$

with $s = 0$ if $p = m, s = 1$ if $p \neq m, \bar{h} = \frac{1}{2}(h + h_q)$ and $\bar{K} = \sum_{i=0}^{\infty} \sum_{j=0}^{\infty} a_{ij} h^{-i} h_q^{-j}$. Again, only several terms are to be calculated. for $h < H_{cr}$, the K's are calculated in terms of the B's, like in (A.10).

C. Orthonormality Relations

There are several orthonormality relations satisfied by the solutions of the Mathieu and modified Mathieu equations which we need. They are listed below:

$$\int_0^{2\pi} d\eta G_m(h,\eta) G_p(h,\eta) = \delta_{mp} N_m(h),$$

$$\int_0^{\xi_0} \int_0^{2\pi} d\xi d\eta (\cosh^2 \xi - \cos^2 \eta) R_{mn} R_{pq} = \delta_{mp} \delta_{nq} M_{mn},$$

$$\int_0^{\infty} \int_0^{2\pi} d\xi d\eta (\cosh^2 \xi - \cos^2 \eta) R_m(h,\xi,\eta) R_p(h',\xi,\eta) = \frac{\pi}{2h} \delta(h - h') \delta_{mp} N_m(h), \quad \text{(A.13)}$$

The function G is Se or So, $R_{mn} = R_m(h_n, \xi, \eta)$, $R_m(h_n, \xi, \eta) = G_m(h, \eta)\ F_m(h, \xi)$, $F_m(h, \xi) = \mathrm{Je}_m(h, \xi)$ or $\mathrm{Jo}_m(h, \xi)$ and ξ_0 is the value of the radial elliptical coordinate ξ at the wall of the hole. At that point and for special values of $h = h_q$, and $h = h_s q, s = 1, 2, 3, \ldots, \mathrm{Je}_{2m}(h_q, \xi_0) = 0$, and $\frac{\partial \mathrm{J}_{e,o_{2m+1}}(h_s, \xi_0)}{\partial \xi} = 0$. These relations are derived from the differential equations 2.7b,c only. Equations are written for different characteristic values, multiplied by appropriate solutions corresponding to any other characteristic value, and summed, subtracted, and integrated by parts, in the process of which some terms drop out due to the boundary conditions. For the relation A.13c we also need the asymptotic forms for Je and Jo (the one following formula A.7). The parts of the quantity M_{mn} containing only periodic solutions can easily be calculated in terms of coefficients B_m, while the parts that contain Je or Jo solutions must by integrated numerically.

ACKNOWLEDGMENT

The authors would like to thank Dan Abell for help with "Mathematica," for the $p = 1$ case.

REFERENCES

[1] R. L. Gluckstern, J. van Zeitz, and B. Zotter, "Coupling impedance of a hole in an elliptical beam pipe," *CERN Preprint SL/AP 92-18.*

[2] R. L. Gluckstern, R. K. Cooper, and R. Li, "Electric polarizability and magnetic susceptibility of small holes in a thin screen," *IEEE Trans. Microwave Theory Tech.*, vol. 38, p. 186, 1990. Correction: vol. 38, p. 1529, 1990.

[3] R. L. Gluckstern, "Coupling impedance of a single hole in a thick wall beam pipe," *CERN Rep. SL/92-05(AP)*, 1992.

[4] S. S. Kurrenoy, "Coupling impedance of pumping holes," particle accelerators, vol. 39, 1992.

[5] S. S. Kurrenoy and G. Stupakov, *SSCL-Preprint 332*, 1993.

[6] A. Chao, "Coherent instabilities of a relativistic bunched beam," *SLAC 1982 Summer School Lectures.*

[7] H. A. Bethe, "Theory of Difraction by Small Holes," *Phys. Rev.*, vol. 66, p. 163, 1944, see also R. E. Collin, *Field Theory of Guided Waves.* New York: McGraw-Hill, 1960.

[8] R. L. Gluckstern and J. A. Diamond, "Penetration of Fields Through a Circular Hole in a Wall of Finite Thickness," *IEEE Trans. Microwave Theory Tech.*, vol. 39, no. 2, 1991.

[9] N. W. McLachlan, *Theory and Appl. of Mathieu Functions.* Oxford Press, 1951.

[10] P. M. Morse and H. Feshbach, *Methods of Theoretical Physics.* New York: McGraw-Hill, 1953.

[11] *Tables Relating to Mathieu Functions, Natl. Bureau of Standards*, 1951.

[12] R. Barakat, A. Houston, and E. Levin, *J. Math. and Phys.*, vol. 42, p. 200, 1963.

[13] W. Press, B. Flannery, S. Teukolski, and W. Vetterling, *Numerical Recepies in C.* Cambridge Univ. Press, 1988.

[14] *Handbook of Mathematical Functions,*M. Abramowitz and I. Stegun, Eds., Natl. Bureau of Standards, 1964.

[15] C. M. Bender and S. A. Orszag, *Advanced Mathematical Methods for Scientists and Engineers.* New York: McGraw-Hill, 1978.

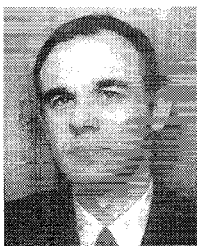

Branislav M. Radak received the B.S. degree in applied physics from the University of Belgrade, Yugoslavia, and the Ph.D. in physics from the University of Maryland in 1991. He is a research associate at the University of Maryland with interests in accelerator physics and nonlinear phenomena.

Robert L. Gluckstern received the B.E.E. degree from the City College of the City University of New York in 1944 and the Ph.D. degree from the Massachusetts Institute of Technology in 1948.

After postdoctoral years at the University of California at Berkely and at Cornell University, he served on the physics faculties of Yale University (1950–1964) and the University of Massachusetts at Amherst (1964–1975). He has been professor of physics at the University of Maryland since 1975, with research interests in the theory in particle accelerators.